

# Applicability of a Representation for the Martin's Real-Part Formula in Model-Independent Analyses

D.A. Fagundes and M.J. Menon  
*Universidade Estadual de Campinas - UNICAMP*  
*Instituto de Física Gleb Wataghin*  
*31083-859 Campinas, SP, Brazil*  
*fagundes@ifi.unicamp.br, menon@ifi.unicamp.br*

Using a novel representation for the Martin's real-part formula without the full scaling property, an almost model-independent description of the proton-proton differential cross section data at high energies (19.4 GeV - 62.5 GeV) is obtained. In the impact parameter and eikonal frameworks, the extracted inelastic overlap function presents a peripheral effect (tail) above 2 fm and the extracted opacity function is characterized by a zero (change of sign) in the momentum transfer space, confirming results from previous model-independent analyses. Analytical parametrization for these empirical results are introduced and discussed. The importance of investigations on the inverse problems in high-energy elastic hadron scattering is stressed and the relevance of the proposed representation is commented. A short critical review on the use of Martin's formula is also presented.

Keywords: Hadron-induced high- and super-high-energy interactions (energy > 10 GeV); elastic scattering.  
 PACS numbers: 13.85.-t, 13.85.Dz.

*Accepted for publication in International Journal of Modern Physics A, 2011*

## Contents

- I. Introduction
- II. Martin's Formula
  - II.A Original Derivation
  - II.B Geometrical Scaling, Developments and Critical Comments
  - II.C A Representation for Almost Model-Independent Analyses
- III. Fit and Results
  - III.A Experimental Data
  - III.B Fit Procedures
  - III.C Results and Comments
- IV. Extracted Overlap and Eikonal Functions
  - IV.A Impact Parameter and Eikonal Representations
  - IV.B Inelastic Overlap Function
  - IV.C Opacity Function in the Momentum Transfer Space
- V. Conclusions and Final Remarks

## I. INTRODUCTION

The theoretical description of the high-energy *elastic* hadron scattering still constitutes a hard challenge for QCD: perturbative techniques cannot be formally applied at this soft (large distances) region and nonperturbative approaches are not yet able to predict *soft scattering states* from first principles without model assumptions [1, 2] some of them unjustified. On the other hand, in the phenomenological context, a wide variety of models can describe the experimental data, but since they are characterized by different physical pictures [3] a comprehensive, well accepted and unified formalism is still missing. This situation has to be contrasted with the great expectations from the new experiments at the CERN LHC, in special the investigation of the soft diffractive processes in proton-proton (*pp*) collisions by the TOTEM Collaboration [4, 5].

At this stage, model-independent analyses, aimed to extract from the experimental data empirical information on what is theoretically unknown, or on what cannot yet be evaluated, may be an important strategy for realistic and necessary developments of the theory in the soft sector. As first steps in that direction, we have investigated the elastic scattering based only on some general principles, high-energy theorems and model-independent fits to the differential cross section data [6–13]. Since the impact parameter and the unitarized eikonal representations still constitutes a useful framework for model developments, the aims have been to extract empirical information on the overlap and eikonal functions (impact parameter and momentum transfer spaces). However, since these analyses demand, as input, experimental information on the differential cross section at intermediate and large values of the momentum transfer, they have been limited to proton-proton scattering in the energy interval 19.4 - 62.5 GeV (as obtained from the CERN SPS, Fermilab and CERN ISR, nearly forty years ago). Therefore, the new data from the LHC on pp collisions at 7 - 14 TeV, covering the region up to large momentum transfer [4, 5] will certainly be crucial for further developments.

One of the main problems with these model-independent analyses is the fact that the phase of the scattering amplitude constitutes a physical observable only in the forward direction (at zero momentum transfer), namely we do not have information on the contributions from the real and imaginary parts of the amplitude beyond the forward direction. As a consequence, if we look for empirical analyses, unbiased by any model/phenomenological ideas [3] different kinds of contributions must be tested and reliable information should not depend, or not strongly depend on the details of these contributions. With this strategy in mind, we have already discussed *two different empirical solutions* for data reductions both statistically consistent [6, 9]. For example, the constrained results obtained in [9] are in agreement with the standart picture, characterized by the dominance of the imaginary part of the amplitude, except at the dip position, where the imaginary part presents a zero (change of sign) and the dip is filled up by the real part. On the other hand, the recent unconstrained results of [6] indicate the dominance of the real part at intermediate values of the momentum transfer, just above the dip region.

Motivated by these different results, both consistent on statistical grounds, we consider here a third possibility with different contributions from those obtained in the above mentioned previous analyses and developed by means of a novel almost model-independent representation for what has been know as Martin's real part formula [14]. This formula connects real and imaginary parts of the elastic scattering amplitude in terms of the transferred momentum in the collision; it has been derived in the context of high-energy theorems and is embodied by a scaling property.

In this work a representation for this formula, without the full scaling property, is used in model-independent analysis of elastic  $pp$  scattering at high energies. By means of an empirical parametrization for the imaginary part of the amplitude, the use of the Martin's formula for the evaluation of the corresponding real part, and fits to  $pp$  differential cross section data (in the interval 19.4 - 62.5 GeV), the overlaps (elastic, inelastic and total) and eikonal functions are extracted in an almost model-independent way. The reproduction of all the experimental data is quite good and the two main results are: the extracted inelastic overlap function (impact parameter space) is characterized by a peripheral effect (tail) above 2 fm and the extracted imaginary part of the eikonal (opacity function) in the momentum transfer space presents a zero (change of sign), in the region 6-7 GeV<sup>2</sup>. Analytical parametrization for these empirical results are introduced and discussed in certain detail.

In the context of our global investigation on the inverse problems in elastic hadron scattering [6, 9] the focus here is only in the foundations, applicability and some consequences of the proposed representation. With this aim we shall only outline references and discussions related to results from previous analyses and phenomenological models. A global critical review, taking into account results that are common to all the analyses (references [6, 9] and those presented here), as well as detailed discussions on the implications in the phenomenological context will be presented in a forthcoming work.

The manuscript is organized as follows. In Sect. II we review the original derivation of the Martin's formula, present some critical comments on subsequent developments and introduce our representation. In Sect. III we describe the fit procedures in some detail and display the results of the data reductions. In Sect. IV we treat the extracted quantities, the inelastic overlap function and the eikonal in the momentum transfer space, making reference to results from previous analysis and some phenomenological models. The conclusions and final remarks are the contents of Sect. V.

## II. MARTIN'S FORMULA

General model-independent properties of the scattering amplitude can be obtained from fundamental principles of local quantum field theory and a set of rigorous theorems [15–18]; in this context, unitarity, analyticity and crossing play a central role. Although rigorous, some results are obtained under specific conditions, which define and limit their range of validity and applicability. Martin's formula has been obtained in this context and therefore it is important to stress the conditions involved. In this Section we first treat the assumptions and main steps in the original derivation [14, 19], followed by a short critical review on the subsequent interpretations and applicability of the formula. After that, we introduce a representation for almost model-independent analysis, with a detailed discussion on the conditions involved.

### A. Original derivation

For elastic processes,  $m + m \rightarrow m + m$ , the laboratory energy  $E$  is a useful crossing symmetry variable. Let  $F$  be the scattering amplitude and  $t$  the square of the momentum transfer. In the high-energy limit ( $E \gg m$ ) the optical theorem reads [20]

$$\sigma_{\text{tot}} = 4\pi \frac{\text{Im}F(E, t=0)}{E},$$

and the Froissat-Martin bound states that [21–23]

$$\sigma_{\text{tot}} \leq C[\ln E]^2,$$

with  $C$  a constant.

In what follows we shall use the symbol  $\sim$  for an asymptotic equality to within a constant factor. Auberson, Kinoshita and Martin [24] (AKM) have shown that if the above bound is saturated ( $\sigma_{\text{tot}} \sim [\ln E]^2$ ), then for

$$|t| < \frac{k}{[\ln E]^2}, \quad k \text{ arbitrary constant}, \quad (1)$$

an scaling property holds

$$\frac{F(E, t)}{F(E, 0)} \rightarrow f(\tau), \quad \tau = t[\ln E]^2 \quad (2)$$

and therefore, in that case, from the optical theorem,

$$F(E, t) \sim E[\ln E]^2 f(t[\ln E]^2).$$

Real and imaginary parts of the amplitude can be correlated through high-energy theorems based on analyticity and the crossing relations established by Bros, Epstein and Glaser in the context of quantum field theory [25, 26]. The main ingredient is the condition of polynomial boundedness and the Phragmén-Lindelöf theorem which leads to the asymptotic uniqueness [27]. By assuming that the odd-under-crossing amplitude can be neglected at high energies, exact crossing for the even (+) amplitude demands that the above real amplitude has structure [19, 27]

$$F_+ \sim iE[\ln E - i\frac{\pi}{2}]^2 f(t[\ln E - i\frac{\pi}{2}]^2).$$

Since  $[\ln E - i\frac{\pi}{2}]^2 \approx [\ln E]^2 - i\pi \ln E$ , the function  $f$  can be expanded and in first order we get

$$f\left(\tau - \frac{i\pi\tau}{\ln E}\right) \approx f(\tau) - \frac{i\pi\tau}{\ln E} \frac{df}{d\tau},$$

so that in the high-energy limit the Martin's result is obtained

$$\text{Im}F_+(E, t) \sim E[\ln E]^2 f(\tau), \quad (3)$$

$$\text{Re}F_+(E, t) \sim \pi E \ln E \frac{d}{d\tau}(\tau f(\tau)). \quad (4)$$

Hence, for a given  $f(\tau)$  (imaginary part), the real part can be evaluated. We stress the four main conditions in this derivation: (1) asymptotic limit (Froissart-Martin bound reached); (2) even amplitude; (3) scaling property; (4)  $|t| < k/[\ln E]^2$ .

## B. Geometrical Scaling, Developments and Critical Comments

“Sometimes these theorems called ‘asymptotic’ are not expected to apply to present available energies, but in fact some of them do apply already now. Then they are no longer theorems but they give useful trends.”

A. Martin, G. Matthiae [19]

In what follows we shall consider the center-of-mass system, with focus in this section on  $pp$  and  $\bar{p}p$  elastic scattering. Let  $A(s, q)$  be the complex amplitude, where  $s$  is the square of the energy and  $q^2 \equiv -t$ . The physical quantities of interest here, with the corresponding normalizations, are the differential cross section

$$\frac{d\sigma}{dq^2} = \pi |A(s, q)|^2, \quad (5)$$

the total cross section

$$\sigma_{\text{tot}} = 4\pi \text{Im}A(s, 0), \quad (6)$$

and the  $\rho$  parameter,

$$\rho(s) = \frac{\text{Re}A(s, 0)}{\text{Im}A(s, 0)}. \quad (7)$$

Martin's result (3-4) was published in 1973, a few months after the introduction of the Geometrical Scaling (GS) by Dias de Deus [28]. This phenomenological approach, further developed by Dias de Deus, Buras and Kroll [29–31] was based on the *empirical evidence* of a scaling in elastic  $pp$  scattering at the ISR energy region ( $\approx 20 - 60$  GeV) in terms of the variables

$$\frac{1}{\sigma_{\text{tot}}^2} \frac{d\sigma}{dq^2} = \Phi(q^2 \sigma_{\text{tot}}). \quad (8)$$

The geometrical aspect concerns the fact that for  $\sigma_{\text{tot}}(s) \propto R^2(s)$ , with  $R(s)$  an effective interaction radius, the increase of the total cross section and all the energy dependence involved in  $d\sigma/dq^2$  is only due to an expansion (geometrical) effect of the hadron.

Now, since from first order derivative dispersion relations [32–34] and for an even amplitude,

$$\rho(s) \approx \frac{\pi}{2\sigma_{\text{tot}}(s)} \frac{d}{d \ln s} \sigma_{\text{tot}}(s), \quad (9)$$

the Martin results, Eqs. (3) and (4), along with normalizations (5), (6) and (7), can be put in the form

$$\frac{d\sigma}{dq^2} = \frac{\sigma_{\text{tot}}^2}{16\pi} \left\{ \left[ \rho \frac{d}{d\tau} [\tau f(\tau)] \right]^2 + [f(\tau)]^2 \right\}, \quad (10)$$

which also characterizes the GS model [29–31], Eq. (8), for  $\tau = q^2 \sigma_{\text{tot}}$  (not necessarily asymptotic energies).

Therefore, the result expressed by Eq. (10) (hereafter referred to as Martin's formula, as in the literature), has two independent foundations:

- (1) the AKM scaling, Eq. (2), a rigorous formal result, deduced under strictly conditions of asymptotic energies (Froissart-Martin bound saturated), valid in a limited interval of momentum transfer, Eq. (1) and for even amplitude;
- (2) the GS, an empirical result verified at the ISR energy region (certainly not asymptotic), without restriction in momentum transfer or crossing properties of the amplitude.

That seems a peculiar and/or accidental fact, putting in evidence some intrinsic difficulties associated with the asymptotic concept and the elastic processes in hadronic interactions, in general, as commented by Martin and Matthiae [19]. Let us shortly review some further developments concerning the energy and momentum transfer variables associated with the Martin's formula.

After the introduction of these scaling in the seventies, the new energy domain reached with subsequent experiments on  $\bar{p}p$  scattering at the CERN  $S\bar{p}pS$  collider (546 GeV) and Fermilab Tevatron (1.8 TeV), have shed light on some aspects involved, as follows. The GS predicts a constant value for the ratio between the elastic and total cross section, a result in agreement with the experimental data at the ISR energy region. However, at the Collider and Tevatron energies it has been verified that this ratio increases [35], leading to the breakdown of the GS. On the other hand, in the phenomenological context, Henzi and Valin have shown that from the ISR to Collider, the energy evolution of the dip-bump structure of the differential cross section demands not only a geometrical expansion but also blackening and edging effects [36, 37]. With their BEL approach (Blacker, Edgier, Larger), based on dispersive diffraction theory, corrections have been introduced in the Martin's formula, leading to extensions at higher energies [38].

Another aspect concerns the interval in momentum transfer in which Eq. (10) is expected or supposed to be valid and that plays a central role in our analysis. In this respect and in the context of the AKM scaling, Kunderát and Lokajíček have developed a detailed numerical analysis [39–41] showing that the function  $f(\tau)$  in (10) is real only in a limited interval of the scaling variable  $\tau$ , corresponding to the region in momentum transfer  $0 \leq q^2 \leq 0.15 \text{ GeV}^2$ . Therefore, the use of the Martin's formula outside this region has no physical meaning. This conclusion, however, has been criticized by Kawasaki, Maehara and Yonezawa [42] and according to these authors, Martin's formula can be directly deduced through derivative dispersion relations in the case that GS holds, which is verified, at least, at the ISR energy region. Therefore, in this energy domain there would be no limit for the applicability of the Martin's formula in terms of the momentum transfer.

Despite the above discussion, a crucial result for our purposes has been introduced by S.M. Roy [43] in the investigation of unitarity inequalities connecting  $\text{Re } A(s, q)$  and  $\text{Im } A(s, q)$ . The main ingredient, suggested by the author and raised by A. Martin (see acknowledgments in [43]), concerns the possibility of a non-scaling only in the imaginary part of the amplitude. In fact, if  $\text{Re } A$  is small compared with  $\text{Im } A$  it seems reasonable to consider the scaling property only in the evaluation of the real part. The proposal by Roy has been to consider Eq. (10) but now with the substitution

$$f(\tau) \Rightarrow g(s, q) = \frac{\text{Im } A(s, q)}{\text{Im } A(s, 0)}. \quad (11)$$

that is, the scaling is supposed to hold only in the small contribution of the real part.

Although under limited formal condition of validity, this proposal can be assumed as a representation for the Martin's formula applicable, in principle, to all values of  $s$  and  $q^2$ . In fact, despite its "hybrid" character the efficacy of this representation in the phenomenological context has been demonstrated, subsequently, by several authors, for both  $pp$  and  $\bar{p}p$  scattering and different regions of the momentum transfer and energy with experimental data available [44–53].

### C. A representation for almost model-independent analyses

As commented in our introduction, motivated by two different model-independent results for the contributions from the real and imaginary parts of the amplitude [6, 9] we consider here a third possibility, based on a representation for the Martin's formula. The point is the Roy's proposal, Eq. (11), with a model-independent parametrization for the imaginary part of the amplitude, in the usual form of a sum of Gaussian in  $q$  (or exponential in  $q^2$ ). Specifically, in Eq. (11) we consider

$$g(s, q) \equiv \sum_{i=1}^n a_i e^{-b_i q^2}, \quad (12)$$

where  $a_i$  and  $b_i$ ,  $i = 1, 2, \dots, n$  are real free parameters. With this assumption and through Eq. (10), we obtain the following representation for the full complex amplitude

$$A(s, q) = \left\{ \left[ \frac{\rho \sigma_{\text{tot}}}{4\pi \sum_{i=1}^n a_i} \right] \frac{d}{dq^2} \left[ q^2 \sum_{i=1}^n a_i e^{-b_i q^2} \right] \right\} + i \left\{ \left[ \frac{\sigma_{\text{tot}}}{4\pi \sum_{i=1}^n a_i} \right] \sum_{i=1}^n a_i e^{-b_i q^2} \right\}. \quad (13)$$

Using as input the experimental values of  $\sigma_{\text{tot}}$  and  $\rho$  in each energy analyzed, we shall consider fits to the differential cross section data through Eqs. (5) and (13). We note that in this representation  $s$  and  $q^2$  are independent variables and the number of free parameters is  $2n - 1$ , due to the constraint

$$\sum_{i=1}^n a_i = 1. \quad (14)$$

However, before considering the above parametrization in our data analysis, some critical comments on its applicability here are in order:

- The analysis by Kundrát and Lokajíček [39–41] concerns the scaling variable  $\tau = q^2 \ln^2 s$  or  $\tau = q^2 \sigma_{\text{tot}}$ . Since in the representation (13) the variables  $s$  and  $q^2$  are independent (Roy's proposal), we understand that the restriction to the narrow interval in the momentum transfer, referred to in Sect. II.B, does not apply.
- As told before, we shall treat only  $pp$  scattering in the energy interval  $19.4 \text{ GeV} \leq \sqrt{s} \leq 62.5 \text{ GeV}$ , a region (ISR) where the GS is empirically verified [54]. Therefore, we see no restriction on its use in the evaluation of the real part of the amplitude.
- On the other hand, just the above energy interval brings about some shortcomings related to formal and practical aspects involved. In fact, at the ISR region,  $pp$  and  $\bar{p}p$  scattering are distinct in what concerns the experimental data on  $d\sigma/dq^2$ ,  $\sigma_{\text{tot}}$  and  $\rho$ . Therefore the neglecting of the odd-crossing amplitude (connected with the asymptotic limit in the Martin's derivation) cannot be justified. Now, even if the odd (-) contribution could be taken into account, that would demand a simultaneous analysis of  $pp$  and  $\bar{p}p$  scattering, since

$$A_{\pm} = \frac{A_{\bar{p}p} \pm A_{pp}}{2}. \quad (15)$$

However, in that case model-independent fits cannot be statistically developed due to the small interval in momentum transfer with data available on  $\bar{p}p$  scattering [12].

Therefore, despite the advantages of parametrization (13), we understand that it has a limited formal justification in what concerns the evaluation of the real part of the amplitude for  $pp$  scattering in the energy interval of interest here. That was the reason why we refer to an almost model-independent analysis.

On the other hand, we stress that we do not intend to extract any direct physical implication or interpretation from the specific contribution of the real part of the amplitude. On the contrary, as commented in the introductory section, our strategy is to look for global properties from different parametrization and fit results that are not connected with or do not strongly depend on the (unknown) contributions from  $\text{Re}A$  and  $\text{Im}A$  beyond the forward direction. With that in mind and as we shall show in the following sections, parametrization (13) brings new useful insights in the investigation of the inverse problems in elastic hadron scattering.

### III. FIT AND RESULTS

Our purpose is to use parametrization (13) to fit differential cross section data through Eq. (5), using as input the experimental values on  $\sigma_{\text{tot}}$  and  $\rho$  in each set analyzed. In this section, we first refer to the data set in which our analysis is based (Sect. III.A), then we discuss the fit procedures in certain detail (Sect. III.B) and after that we present the fit results and some critical comments (Sect. III.C).

### A. Experimental data

In the context of our empirical analyses [6–13], the evaluation of the uncertainties in the extracted quantities plays a central role. Since the fits are based on the differential cross sections, that demands sets with available data covering the largest intervals in momentum transfer, mainly in what concerns the region of high momentum transfer. As already discussed in some detail [6, 9, 12] this condition limits the analysis to six sets of  $pp$  elastic scattering data, at  $\sqrt{s} = 19.4$  GeV (from the Fermilab and CERN SPS) and  $\sqrt{s} = 23.5, 30.7, 44.7, 52.8$  and  $62.5$  GeV (from the CERN ISR). In addition, we make use of the empirical result that at the ISR energy region (23.5 - 62.5 GeV) the differential cross section data above  $q^2 \sim 4$  GeV<sup>2</sup> do not depend on the energy [55–58]. This fact allows the inclusion in each set (ISR) the data at 27.4 GeV (from Fermilab), covering the large momentum transfer region:  $5.5 \leq q^2 \leq 14.2$  GeV<sup>2</sup> (see [9] for a quantitative discussion on this respect).

The data set have been collected from final published results and a complete list of references, with comments, can be found in [6] for the data at 19.4 GeV and in [9] for the ISR data (23.5 - 62.5 GeV). The differential cross sections data include the optical point,

$$\left. \frac{d\sigma}{dq^2} \right|_{q^2=0} = \frac{\sigma_{\text{tot}}^2(1 + \rho^2)}{16\pi} \quad (16)$$

and the data above the Coulomb-nuclear interference region,  $q^2 > 0.01$  GeV<sup>2</sup>. All the available data have been included, without any kind of selection or exclusion of data points. As a test for goodness of fit we shall consider the  $\chi^2$  per degrees of freedom (DOF) and since this test is based on the assumption of a Gaussian error distribution, only the statistical errors of the experimental data are taken into account (we do not include systematic errors). We shall return to this point in our comments at the end of Sect. III.C.

### B. Fit procedures

The data reductions have been performed using the CERN-Minuit code [59] through successive runs of the MIGRAD minimizer and with the confidence level for the uncertainties in the free parameters fixed at 70 % . The nonlinearity of the fit demands the start values of the free parameters and looking for a completely unbiased procedure the following methodology has been used.

We have begun the analysis with the differential cross section set corresponding to the largest experimental information available, namely  $\sqrt{s} = 52.8$  GeV (plus data at 27.4 GeV, as explained in Sect. III.A) and through the following steps:

1. First we have considered only the optical point and the data in the narrow interval  $0.01 < q^2 \leq 0.1$  GeV<sup>2</sup> (very forward direction). In the logarithmic scale, the differential cross section data follows a well defined straight line, so that the slope and the intercept can be directly evaluated from the plot and used as start values for the fit with only one exponential term in parametrization (13), that is,  $n = 1$ .
2. Once obtained the final fit result, we have enlarged the interval up to  $q_{\text{max}}^2 = 0.2$  GeV<sup>2</sup>. Due to a sudden change of the slope around 0.13 GeV<sup>2</sup>, we have considered two exponential terms ( $n = 2$ ) and used as start values for the parameters in both terms the final values of the previous fit. With this procedure the break of the slope is quite well described, as well as all the data in the above interval.
3. Next we have considered  $q_{\text{max}}^2 = 0.5$  GeV<sup>2</sup> and this case demands  $n = 3$ . As start values for the third exponential terms we have tested the final values of each of the two terms in the previous step and selected the best result (reduced  $\chi^2$  closest to 1).
4. The same procedure has been then applied for  $q_{\text{max}}^2 = 1.0, 2.0, 3.0, 4.0$  GeV<sup>2</sup> and after that,  $q_{\text{max}}^2 = 14.2$  GeV<sup>2</sup>.

Once obtained the best result at 52.8 GeV, the final values of the parameters have been used as feed back for the fits at each nearby energy set, namely from 52.8 GeV to 62.5 GeV, from 52.8 GeV to 44.7 GeV and then from 44.7 GeV to 30.7, 23.5 and 19.4 GeV, successively.

TABLE I: Fit results for each data set and statistical information: degrees of freedom (DOF) and reduced chi square ( $\chi^2/\text{DOF}$ ). For  $i=1,2,\dots,6$ , the parameters  $a_i$  are dimensionless and  $b_i$  in  $\text{GeV}^{-2}$ .

$\sqrt{s}$ (GeV):	19.4	23.5	30.7	44.7	52.8	62.5
$a_1$	0.111 $\pm 0.011$	0.506 $\pm 0.029$	0.333 $\pm 0.019$	0.0791 $\pm 0.0097$	0.151 $\pm 0.017$	0.179 $\pm 0.022$
$a_2$	5.150 $\pm 0.014$	5.734 $\pm 0.032$	5.740 $\pm 0.023$	5.825 $\pm 0.017$	6.8323 $\pm 0.018$	6.7449 $\pm 0.019$
$a_3$	-8.4565 $\pm 0.016$	-8.4602 $\pm 0.033$	-8.4491 $\pm 0.024$	-8.444 $\pm 0.017$	-7.5697 $\pm 0.018$	-7.6620 $\pm 0.019$
$a_4$	-0.985 $\pm 0.011$	-0.00665 $\pm 0.00085$	-0.0089 $\pm 0.0011$	-0.0099 $\pm 0.0012$	-0.00862 $\pm 0.00082$	-0.0064 $\pm 0.0012$
$a_5$	-0.00165 $\pm 0.00010$	-0.000142 $\pm 0.000069$	-0.000271 $\pm 0.000090$	-0.00037 $\pm 0.00011$	-0.00023 $\pm 0.000075$	-0.000203 $\pm 0.000093$
$a_6$	5.187 $\pm 0.017$	3.219 $\pm 0.036$	3.384 $\pm 0.027$	3.564 $\pm 0.018$	1.598 $\pm 0.019$	1.742 $\pm 0.020$
$b_1$	14.7 $\pm 1.7$	7.82 $\pm 0.45$	9.56 $\pm 0.60$	31.3 $\pm 5.8$	16.4 $\pm 1.8$	14.1 $\pm 1.7$
$b_2$	3.2466 $\pm 0.0045$	3.3610 $\pm 0.0061$	3.3095 $\pm 0.0040$	4.1790 $\pm 0.0085$	3.9811 $\pm 0.0068$	3.786 $\pm 0.013$
$b_3$	3.7449 $\pm 0.0045$	3.4191 $\pm 0.0033$	3.4232 $\pm 0.0083$	4.4031 $\pm 0.0078$	4.0619 $\pm 0.0069$	3.852 $\pm 0.013$
$b_4$	2.7230 $\pm 0.0095$	1.004 $\pm 0.055$	1.150 $\pm 0.057$	1.242 $\pm 0.067$	1.156 $\pm 0.046$	1.079 $\pm 0.079$
$b_5$	0.5993 $\pm 0.0084$	0.373 $\pm 0.046$	0.433 $\pm 0.036$	0.469 $\pm 0.035$	0.426 $\pm 0.036$	0.418 $\pm 0.046$
$b_6$	4.277 $\pm 0.010$	3.610 $\pm 0.015$	3.8146 $\pm 0.013$	5.121 $\pm 0.025$	5.1138 $\pm 0.057$	4.756 $\pm 0.078$
DOF	302	161	200	235	233	152
$\chi^2/\text{DOF}$	3.00	1.59	1.42	2.11	1.74	1.23

As described above, we did not impose any kind of constraint in the fit procedure, in special in what concerns the number of parameters or possible dependencies of the parameters with the energy. The only goal has been to obtain the best fit on statistical grounds.

### C. Results and Comments

The final values of the free parameters and statistical information on the fit results for each set analyzed are displayed in Table I. With the Minuit code, the error-matrix provides the variances and covariances associated with each free parameter. This information, together with the statistical errors of  $\sigma_{\text{tot}}$  and  $\rho$ , are used in the evaluation of uncertainty regions in the differential cross section and all the extracted quantities, through standard error propagation procedures [60]. The results together with the corresponding experimental data are shown in Fig. 1 in all the  $q^2$  region and at the diffraction peak. The contributions to the differential cross sections from the real and imaginary parts of the amplitude,

$$\frac{d\sigma^R}{dq^2} = \pi [\text{Re } A]^2, \quad \frac{d\sigma^I}{dq^2} = \pi [\text{Im } A]^2, \quad (17)$$

are shown in Fig. 2, where we display only the uncertainty regions and the experimental data.

Before considering the extracted quantities some comments on the fit results presented in this section are in order, as follows.

From Table I, although the values of each parameter in each one of the six sets analyzed are practically of the same order of magnitude, a dependence on the energy cannot be inferred. That is a consequence of our fit procedure, developed without any kind of constraint in the free parameters, as well as the relatively small energy interval investigated ( $\approx 19 - 60$  GeV). In fact, the same undefined energy dependence on the free parameters characterizes the results in our previous analyses, with both the constrained [9] and unconstrained [6] parametrization. In this respect, the new data on the

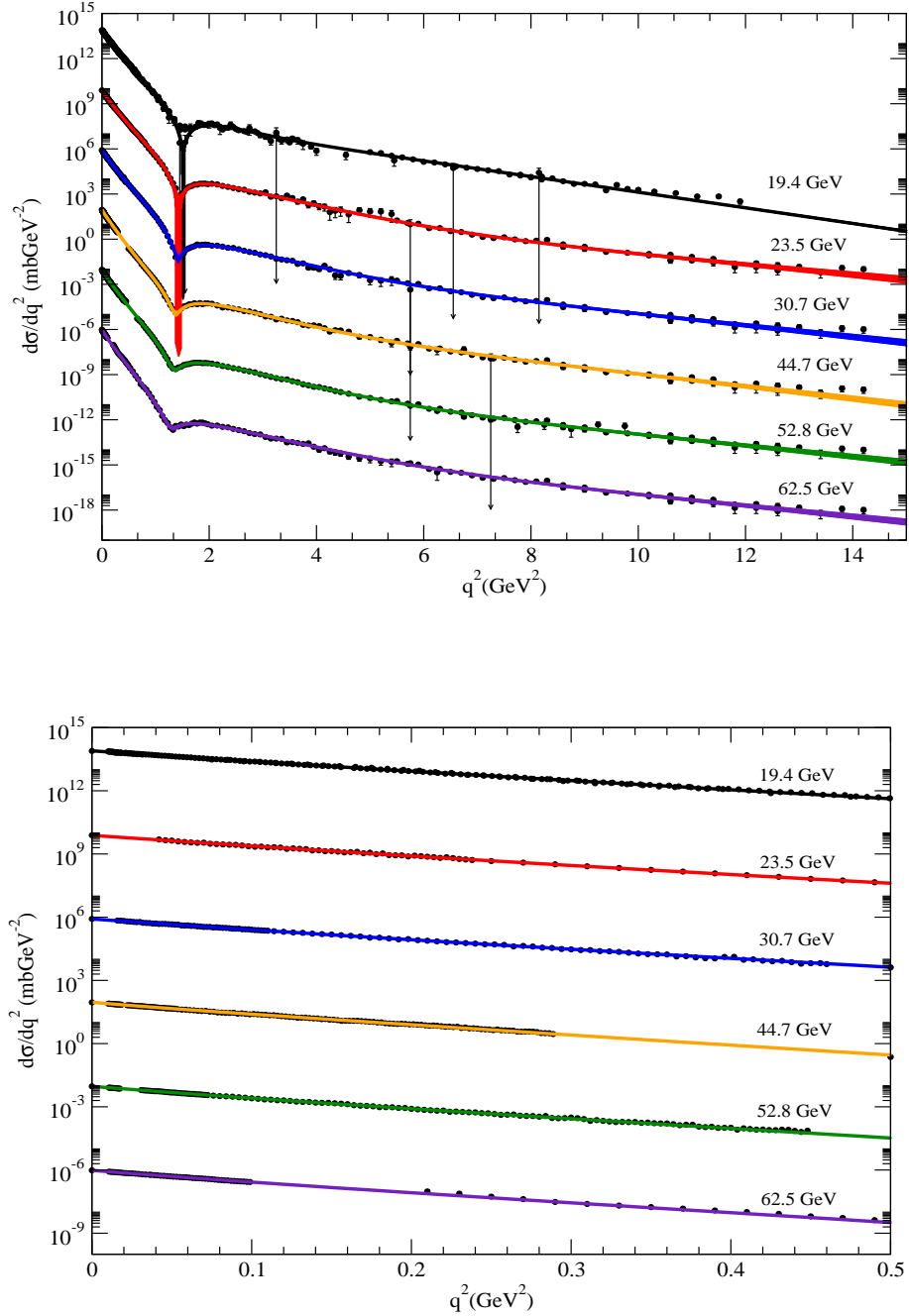


FIG. 1: Fit results and uncertainty regions from error propagation: all  $q^2$  region (above) and diffraction peak (below). Curves and data have been multiplied by factors of  $10^{\pm 4}$ .

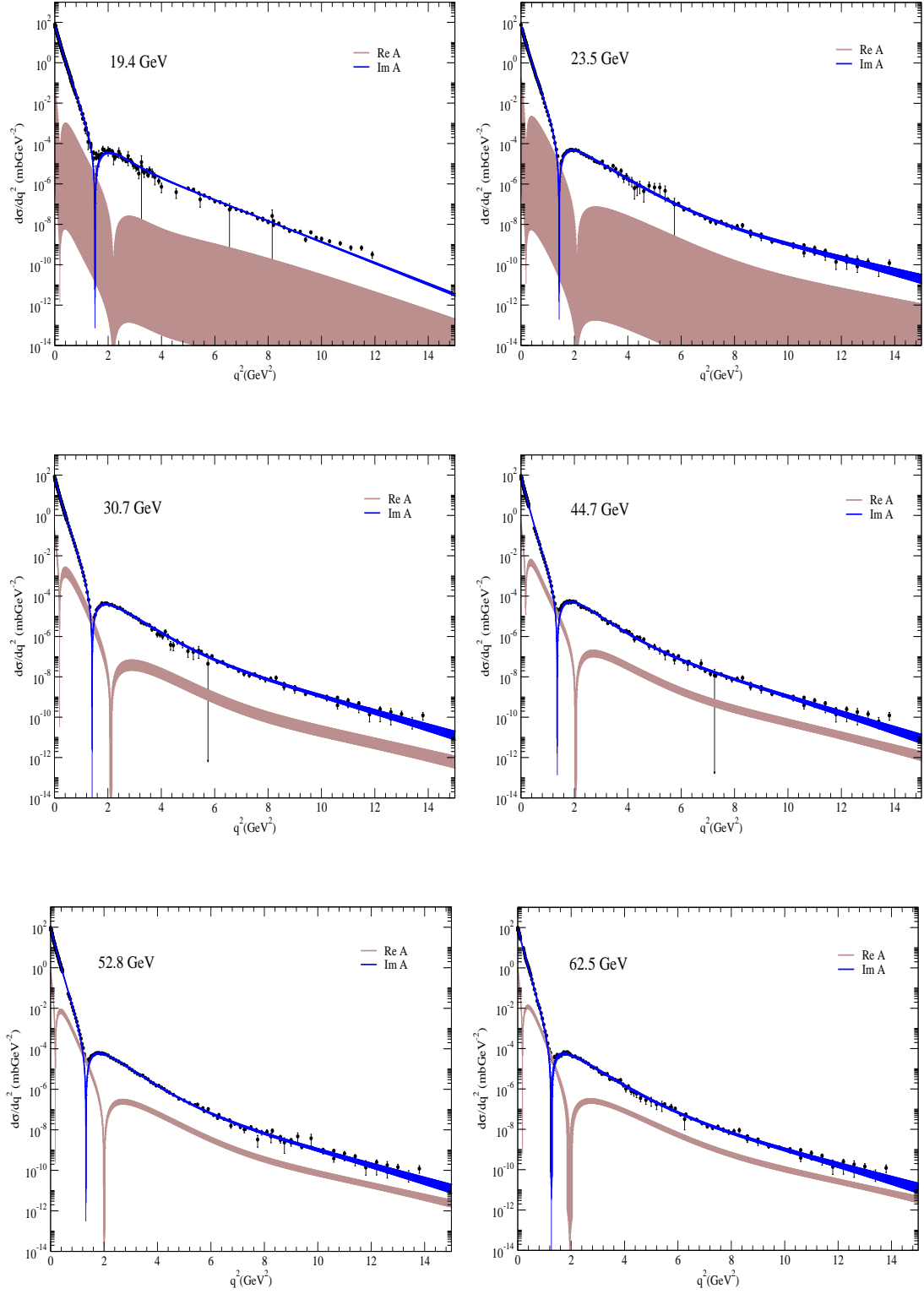


FIG. 2: Experimental data and uncertainty regions in the contributions to the differential cross sections from the real (gray) and imaginary (black) parts of the amplitude.

differential cross section from the LHC (7 - 14 TeV) reaching the large momentum transfer region may bring important information for further investigation on possible energy dependencies.

Although Figure 1 shows that all the experimental data are quite well described, from Table I we note that the values of the  $\chi^2/\text{DOF}$  for about 200 DOF correspond to extremely small confidence intervals. That is a consequence of the fact that we have considered only statistical errors and not the systematic ones. The inclusion of the systematic errors (for example in quadrature with the statistical ones) lead to quite good confidence intervals, but we do not think this procedure has statistical meaning, as commented at the end of in Sect. III.A.

From the plots in Figure 2, the contributions to the differential cross section from Re  $A$  and Im  $A$  are in agreement with the standard or generally expected behavior: dominance of the contribution from Im  $A$  except at the dip region, which is filled up by the contribution from Re  $A$ . In all sets Im  $A$  present a zero (change of sign) at the dip position and Re  $A$  two zeros, one at small values of the momentum transfer (in accordance with a theorem by A. Martin for even amplitudes [61]) and another one around  $q^2 = 2 \text{ GeV}^2$ . We also note that the large uncertainty regions associated with Re  $A$ , as compared with those from Im  $A$ , are consequence of the derivative term in parametrization (13) and the variances/covariances involved. Also, from the plots we see that the uncertainty regions from Re  $A$  are larger at the lower energies, which is explained by our fit procedure that started at 52.8 GeV, and also the derivative term referred to above.

At last it should be noted that some characteristics of the fit results here presented and also of those in our previous empirical analysis [6, 9] are consequences of the data ensemble considered, the choice of the analytical parametrization as sum of exponential in  $q^2$  and the use of statistical errors only and not systematic ones. In this respect three comments are in order as follows.

(1) All our analyses have been based on the addition of the data at 27.4 GeV to the five ISR sets (23.5 - 62.5 GeV). The empirical justification for this procedure has been discussed in detail by Ávila and Menon in [9], Sect. 3.3.2. Specifically, by testing different cutoffs in the momentum transfer, it has been verified that for  $q^2 \geq 3.5 \text{ GeV}^2$  all the above differential cross section data follows a power law in  $q^2$  with power  $\lambda = -7.85 \pm 0.04$  [9], indicating therefore an energy-independent behavior of the differential cross section in this kinematic region. On the other hand, in the QCD context, it is expected that this region of large momentum transfer in elastic scattering may be accessed by perturbative techniques. In this respect the above result favors the triple-gluon exchange picture by Donnachie and Landshoff [57, 58], which predicts  $\lambda = -8$ , but not the constituent interchange model (CIM) by Lepage and Brodsky [62], since in this case it is predicted  $\lambda = -10$ . This approach also predicts a scaling of the form

$$\frac{d\sigma}{dq^2} \sim s^{-10} f\left(\frac{q^2}{s}\right),$$

which has been verified at lower energies [62]. There is also indication of agreement with the data at 19.4 GeV and 27.4 GeV, if a particular power law is assumed for  $f(q^2/s)$  and the systematic uncertainties of 15% present in both sets are neglected [56]. This small energy dependence in the interface between Fermilab and ISR energies corroborates the analysis by Ávila and Menon in the sense to include the data at 27.4 GeV only at the ISR sets and not at 19.4 GeV (see [9], Sect. 3.3.2, for more details).

(2) Another aspect in our analyses concerns the assumption of a sum of exponential in  $q^2$ , for the *whole* range of momentum transfer investigated. This choice has two foundations as follows. The first one is strictly empirical since for the differential cross sections in a logarithm scale all the details of the diffraction peak, the dip-bump structure and the large  $q^2$  region can be well described by compositions of straight lines, analogous to an exhaustion process (the empirical character of our analysis impose no limits in the number of free parameters or exponential terms). The second one, to be treated in the next section, concerns the possibility of *analytical* translation from the  $q^2$ -space to the impact parameter space (Fourier transform) and, more importantly, the *analytical* evaluation of the uncertainties in some extracted quantities, through error propagation from the fit parameters. On the other hand, as referred to above, the justification for the inclusion of the data at 27.4 GeV to the ISR sets was based on a power law fit analysis at the large momentum transfer region and not exponential forms. In this respect, it should be noted that as the momentum transfer increases, a replacement of an exponential decrease of the differential cross section to a power one may be related to a transition from soft to hard sectors and in the phenomenological context can be connected with the geometrical structure of the Regge trajectories, from linear to non-linear one, respectively, as discussed by Fiore

*et al.* [3] (Sect. 6). Therefore, it might also be important to investigate the possibility to combine exponential and power forms in an unique analytical parametrization. However, we shall limit our analyses to exponential forms for the reasons referred to above, namely they represent a suitable empirical ansatz, “unbiased by any theoretical prejudice”, as suggested by Fiore *et al.* [3] and allows analytical translation to the impact parameter space.

(3) The last aspect concerns the dataset considered [6, 9] and the use of statistical errors only and not systematic ones. In this respect it should be noted that another data sets exist, as that compiled and analyzed by Cudell, Lengyel and Martynov [63] (where the systematic errors are taken into account) and available in [64]. We think it would also be interesting to develop new data reductions with this data set and our proposed parametrization; a comparative analysis on all the results could be useful.

#### IV. EXTRACTED OVERLAP AND EIKONAL FUNCTIONS

In this section we consider some implications of the fit results in what concerns properties of the extracted overlap functions and the imaginary part of the eikonal (opacity) in the momentum transfer space. We first recall the main formulas associated with the impact parameter and eikonal representations (Sect. IV.A) and then discuss in some detail the extracted inelastic overlap function (Sect. IV.B) and the opacity function in the momentum transfer space (Sect. IV.C).

##### A. Impact Parameter and Eikonal Representations

This subject is treated in detail in [1]. In what follows we only recall the main formulas of interest here.

The representation of the elastic scattering amplitude in the impact parameter space is named profile function and in case of azimuthal symmetry they are connected by

$$A(s, q) = i \int_0^\infty b db J_0(qb) \Gamma(s, b), \quad (18)$$

where  $b$  is the impact parameter,  $\Gamma(s, b)$  the profile function and  $J_0$  is the zero-order Bessel function. In the eikonal representation the profile is given by

$$\Gamma(s, b) = 1 - e^{i\chi(s, b)}, \quad (19)$$

where  $\chi(s, b)$  is the eikonal function.

The unitarity principle in the impact parameter space is usually expressed in terms of the total, elastic and inelastic overlap functions,

$$G_{\text{tot}}(s, b) = G_{\text{el}}(s, b) + G_{\text{in}}(s, b), \quad (20)$$

which, in terms of the profile function reads

$$2\text{Re}\Gamma(s, b) = |\Gamma(s, b)|^2 + G_{\text{in}}(s, b), \quad (21)$$

where  $G_{\text{in}}(s, b)$  is the inelastic overlap function and it follows that the integrated inelastic cross section is given by

$$\sigma_{\text{in}}(s) = 2\pi \int_0^\infty b db G_{\text{in}}(b, s). \quad (22)$$

In the eikonal representation, from Eqs. (19) and (21),

$$G_{\text{in}}(s, b) = 1 - e^{-2\text{Im}\chi(s, b)}. \quad (23)$$

Since unitarity implies  $\text{Im}\chi(s, b) \geq 0$  we have  $G_{\text{in}}(s, b) \leq 1$ , so that from (22)  $G_{\text{in}}$  can be interpreted as the probability of an inelastic event to take place at given  $b$  and  $s$ ; in the black disk limit  $G_{\text{in}} \rightarrow 1$ .

From the above result, the imaginary part of the eikonal is associated with the absorption in the scattering process and for that reason is named *opacity function*, which we shall denote

$$\Omega(s, b) \equiv \text{Im}\chi(s, b). \quad (24)$$

In the momentum transfer space it is given by the symmetrical Fourier-Bessel transform, with notation

$$\tilde{\Omega}(s, q) = \int_0^\infty b db J_0(qb) \Omega(s, b). \quad (25)$$

Eikonal models can be classified or distinguished according to different choices for the opacity function in the momentum transfer space, which is expected to be connected with form factors and elementary amplitudes.

Due to the importance of the physical interpretations associated with the *inelastic overlap function* and the *opacity function in the momentum transfer space*, we shall display and discuss these extracted quantities from the fit results. However, before that, we stress again that the relatively small interval investigated ( $\approx 19 - 60$  GeV) and the unconstrained fit procedure, turn out difficult to infer energy dependencies on these quantities since, in general, the error propagation leads to an overlapping of the uncertainty regions. We understand that this does not constitute a serious drawback in our analyses because in the phenomenological context what is theoretically unknown, in general, concerns the impact parameter and momentum transfer distributions and not the dependencies on the energy [1–3]. Therefore we shall limit the results to typical cases of interest at fixed energy, or those for which there is no overlapping of the uncertainties.

## B. Inelastic Overlap Function

With parametrization (13), the profile function can be *analytically evaluated* through the inverse (symmetrical) transform of Eq. (18),

$$\Gamma(s, b) = -i \int_0^\infty q dq J_0(qb) A(s, q), \quad (26)$$

as well as the overlap functions in Eqs. (20) and (21), together with the associated uncertainties through error propagation. For each  $b$ -interval considered for the extracted quantities, we have generated  $10^3$  empirical points in the form of a central value and the corresponding uncertainty, namely  $G \pm \Delta G$ .

The results for the extracted overlap functions in all the energies investigated are very similar and are illustrated in Fig. 3 in the case of  $\sqrt{s} = 52.8$  GeV (largest set of experimental data). The figure, in linear scale, shows the uncertainty regions for the extracted total, elastic and inelastic overlap functions. We note that at  $b = 0$ ,  $G_{\text{in}}$  reaches  $\approx 92\%$  of the black disc limit, as expected [65, 66].

We now focus on the extracted inelastic overlap function. In order to develop some test on the reliability of the extracted results, we have evaluated the integrated inelastic cross section through Eq. (22), a quantity that was not used as experimental input in the data reductions. The results for all the sets analyzed are displayed in Table II, showing plenty agreement with the corresponding experimental data. The data at 19.4 GeV has been evaluated from  $\sigma_{\text{tot}} = 38.98 \pm 0.04$  mb obtained by Carroll *et al.* [67] and  $\sigma_{\text{el}} = 6.78 \pm 0.13$  mb by Schiz *et al.* [68]. Those at the ISR region come from the analysis by Amaldi and Schubert [54].

Next, let us discuss the structure of  $G_{\text{in}}$  in the impact parameter space. The result at  $\sqrt{s} = 52.8$  GeV, in the form of points with errors and in a logarithm scale, is displayed in Figure 4. First we note that in the region 0 - 2 fm the empirical points follow a Gaussian dependence with center at the origin, but above this region the decrease is slower and deviate from the Gaussian in the form of a tail. This effect is not new since it has already been observed by Amaldi and Schubert [54] and also Henyey, Tuan and Kane [69] in the seventies. In terms of the differential cross section data it is connected with the change of the slope at  $\approx 0.13$  GeV<sup>2</sup>, referred to in Sect. III.B.

In order to go further, looking for some quantitative information on this tail effect, we have tested different analytical parametrization for the empirical points in Fig. 4 and in this case we have also considered all the energies investigated. Making use of the CERN-Minuit code and using as test

TABLE II: Integrated inelastic cross section evaluated through Eq. (22) with the extracted inelastic overlap functions and the experimental data [54, 67, 68].

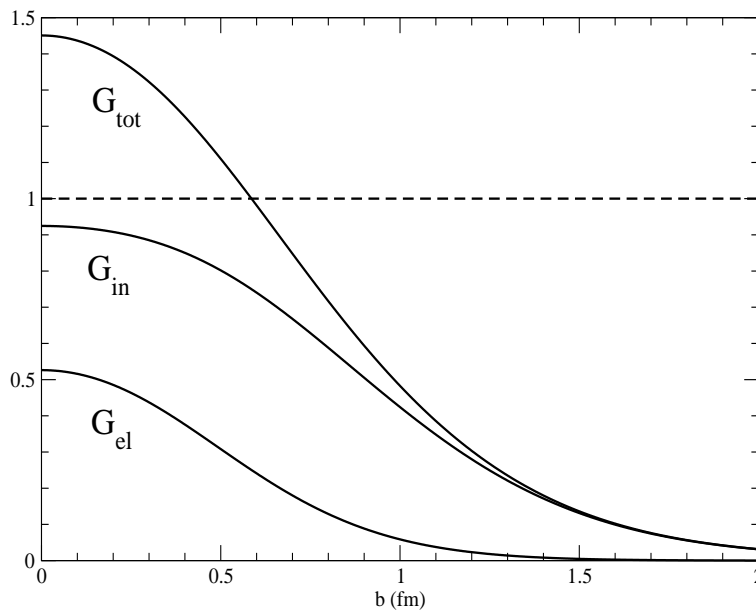
$\sqrt{s}$ (GeV)	$\sigma_{in}^{fit}$ (mb)	$\sigma_{in}^{exp}$ (mb)
19.4	32.03±0.04	32.11±0.14
23.5	32.21±0.16	32.21±0.14
30.7	32.99±0.13	32.98±0.14
44.7	34.62±0.11	34.62±0.14
52.8	35.23±0.13	35.22±0.16
62.5	35.64±0.16	35.66±0.21

functions exponential, Gaussian and combinations of these functions, the best global result has been obtained with a composition of three Gaussian, which we shall denote

$$G_{in}(b) = \sum_{i=1}^3 A_i e^{-B_i(b-C_i)^2} = \sum_{i=1}^3 G_i(b), \quad (27)$$

where  $A_i$ ,  $B_i$  and  $C_i$ ,  $i = 1, 2, 3$  are free fit parameters. The result of the fit, through the CERN-Minuit code, for  $pp$  at 52.8 GeV is shown in Fig. 4, together with the corresponding components  $G_i(b)$ ,  $i = 1, 2, 3$ ; the values of the parameters are displayed in Table III. In this case, since the ensemble corresponds to extracted empirical points with errors and not to experimental data we did not evaluate the uncertainties associated with these components and make no reference to the goodness of fit (reduced  $\chi^2$ ).

The results for each Gaussian component,  $G_i$ ,  $i = 1, 2, 3$ , in each energy investigated are displayed in Fig. 5. Although, once more, a dependence on the energy cannot be extracted in this interval, we can identify the following remarkable features: (1) each component is concentrated in specific regions of the impact parameter space, with centers at  $b = 0$  ( $G_1$ ), around  $b = 0.6$  fm ( $G_2$ ) and roughly

FIG. 3: Uncertainty regions of the extracted overlap functions for  $pp$  scattering at 52.8 GeV and the black disc limit (dashed line).

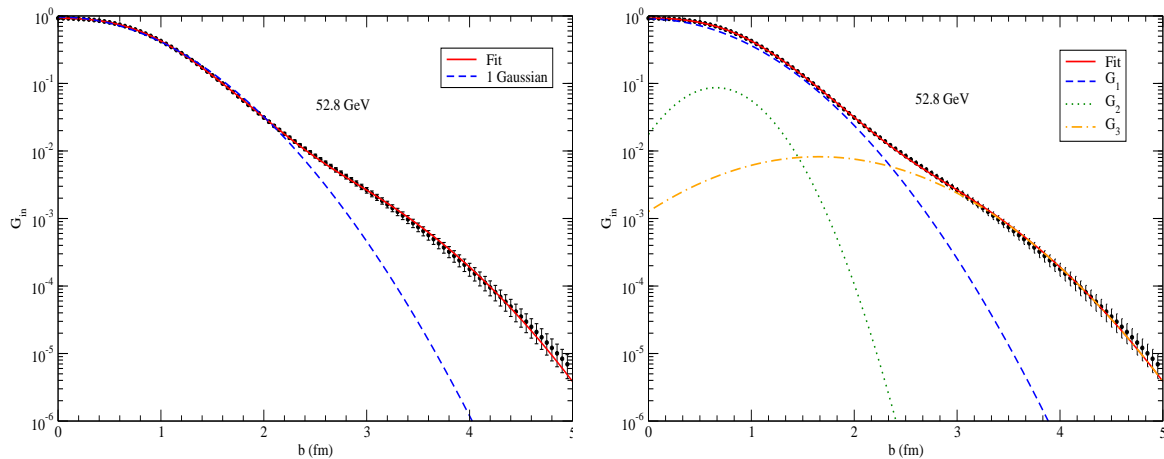


FIG. 4: Extracted points with uncertainties for the inelastic overlap function at 52.8 GeV. Left: fit with one Gaussian centered at the origin (dashed) and parametrization (27) (solid). Right: result of the fit and the three Gaussian components in Eq. (27).

TABLE III: Fit results for the Gaussian components of the inelastic overlap function, Eq. (27) at 52.8 GeV.

$i$	$A_i$	$B_i$ ( $\text{fm}^{-2}$ )	$C_i$ ( $\text{fm}$ )
1	$0.9005 \pm 0.0067$	$0.908 \pm 0.020$	$0.0 \pm 0.0$
2	$0.0866 \pm 0.0048$	$3.71 \pm 0.32$	$0.655 \pm 0.015$
3	$0.00821 \pm 0.00020$	$0.684 \pm 0.024$	$1.653 \pm 0.034$

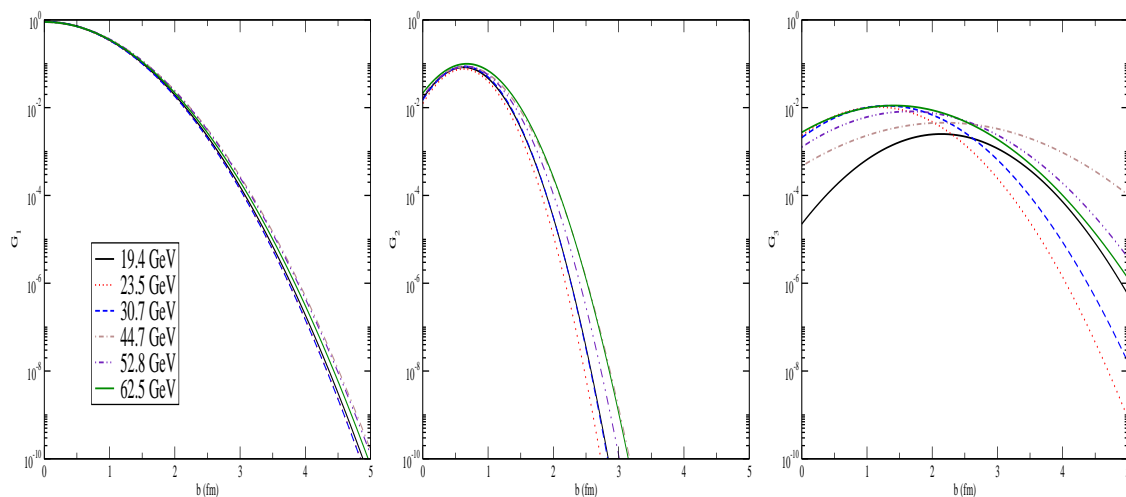


FIG. 5: Gaussian components of the inelastic overlap function, Eq. (27), for each set analyzed. Solid lines correspond to the extrem energies (19.4 and 62.5 GeV) and the other symbols to the intermediate energies.

TABLE IV: Contribution from each Gaussian component to the integrated inelastic cross section and the sum of the contributions.

$\sqrt{s}$ (GeV)	$\sigma_{\text{in}}^{G_1}$ (mb)	$\sigma_{\text{in}}^{G_2}$ (mb)	$\sigma_{\text{in}}^{G_3}$ (mb)	$\sum_{i=1}^3 \sigma_{\text{in}}^{G_i}$ (mb)
19.4	29.67	2.87	0.59	33.13
23.5	29.02	2.48	1.29	32.79
30.7	29.23	3.01	1.63	33.87
44.7	31.02	3.52	1.60	36.14
52.8	31.15	3.31	1.84	36.30
62.5	30.26	4.26	2.12	36.49

around  $b = 2.0$  fm ( $G_3$ ); (2)  $G_1$  dominates the central and intermediate regions and  $G_3$  describes the tail effect above  $b \approx 2.2$  fm; (3) the effect of different energies is more evident in  $G_3$  than in the others components.

In order to get some quantitative information on the relative contribution of each Gaussian component in the integrated cross section, we have evaluated the following partial quantities:

$$\sigma_{\text{in}}^{G_i}(s) = 2\pi \int_0^\infty b db G_i(b, s), \quad i = 1, 2, 3. \quad (28)$$

The results with the corresponding sum of the partial contributions in each energy are shown in Table IV. Certainly this sum of the areas under the curves cannot be identified with  $\sigma_{\text{in}}$ , but allows to infer that, roughly, the relative contributions read 85 % from  $G_1$ , 10 % from  $G_2$  and 5 % from  $G_3$ . Moreover, from Table IV, in this energy interval the relative errors associated with the average of each contribution, namely  $\Delta < \sigma_{\text{in}}^{G_i} > / < \sigma_{\text{in}}^{G_i} >$ , correspond to 3%, 19% and 35% for  $i = 1, 2, 3$  respectively. These quantitative results can be interpreted as evidence that the peripheral region is more sensitive to variations of the energy than the intermediate region and this one yet more sensitive than the central region. That seems a reasonable result, since we are treating the inelasticity associated with the elastic channel through unitarity. Also, from Table IV we can see that except for the result at 44.7 GeV, the contribution from  $G_3$  increases with the energy.

In conclusion, these results indicate three Gaussian components for the inelastic overlap function associated with central, intermediate and peripheral regions. Although an explicit dependence on the energy cannot be obtained the results suggest that the peripheral region is more sensitive to the energy evolution than the central region. We understand that the correct evaluation of  $\sigma_{\text{in}}$  (Table II) and the reproduction of the tail effect in  $G_{\text{in}}$  give support to our representation and fit procedure.

### C. Opacity Function in the Momentum Transfer Space

With the extracted profile function we determine the opacity function in the impact parameter space *analytically*, through Eqs. (19) and (24),

$$\Omega(s, b) = \ln \left\{ \frac{1}{\sqrt{[1 - \text{Re} \Gamma(s, b)]^2 + [\text{Im} \Gamma(s, b)]^2}} \right\}, \quad (29)$$

together with the corresponding uncertainties by error propagation from the fit parameters.

Now, since  $\Gamma(s, b)$ , from  $A(s, q)$  in (13), is given by a sum of Gaussian in  $b$ , the translation to  $q^2$ -space, through Eq. (25), cannot be analytically performed and therefore the error propagation neither. For that reason we have used the semi-analytical approach discussed by Ávila and Menon [9] which is valid under certain condition (as explained in what follows) and that we shall name *conditioned expansion method*.

From the fit results and in all the energies analyzed, we have found that

$$\left[ \frac{\text{Im} \Gamma(s, b)}{1 - \text{Re} \Gamma(s, b)} \right]^2 \equiv r(s, b) \ll 1, \quad (30)$$

including the uncertainty regions. This is illustrated in Fig. 6 in the typical case of  $\sqrt{s} = 52.8$  GeV. Therefore, Eq. (29) for the opacity can be approximated by

$$\Omega(s, b) \approx \ln \left\{ \frac{1}{1 - \text{Re}\Gamma} \right\}. \quad (31)$$

In order to avoid loss of information, we look for what can be directly obtained from the fit. In this case, by adding and subtracting  $\text{Re}\Gamma$ , the above equation can be expressed by

$$\Omega(s, b) = \text{Re}\Gamma(s, b) + R(s, b), \quad (32)$$

where the “residual” function is given by

$$R(s, b) = \left[ \ln \left\{ \frac{1}{1 - \text{Re}\Gamma} \right\} - \text{Re}\Gamma(s, b) \right]. \quad (33)$$

Now, the Fourier-Bessel transform of (32) reads

$$\tilde{\Omega}(s, q) = \text{Im}A(s, q) + \tilde{R}(s, q), \quad (34)$$

so that the first term is directly obtained from the fit and the residual function can be determined through a *semi-analytical method* [9]. Specifically, with (33) we generate a set of points with errors (from propagation),  $R_i(s, b) \pm \Delta R_i(s, b)$ ,  $i = 1, 2, \dots, N$  and parametrize this set by Gaussian forms,

$$R(s, b) = \sum_{j=1}^m A_j e^{-B_j b^2}, \quad (35)$$

which has analytical Fourier-Bessel transform and allows error propagation. Then, substitution in (34), together with  $\text{Im}A$  from the fit, leads to  $\tilde{\Omega}(s, q) \pm \Delta\tilde{\Omega}(s, q)$ .

Following the procedure by Ávila and Menon [9] we display the results in terms of  $q^8$  multiplied by  $\tilde{\Omega}(q)$  together with the uncertainty regions, as shown in Fig. 7 for all sets investigated. A remarkable

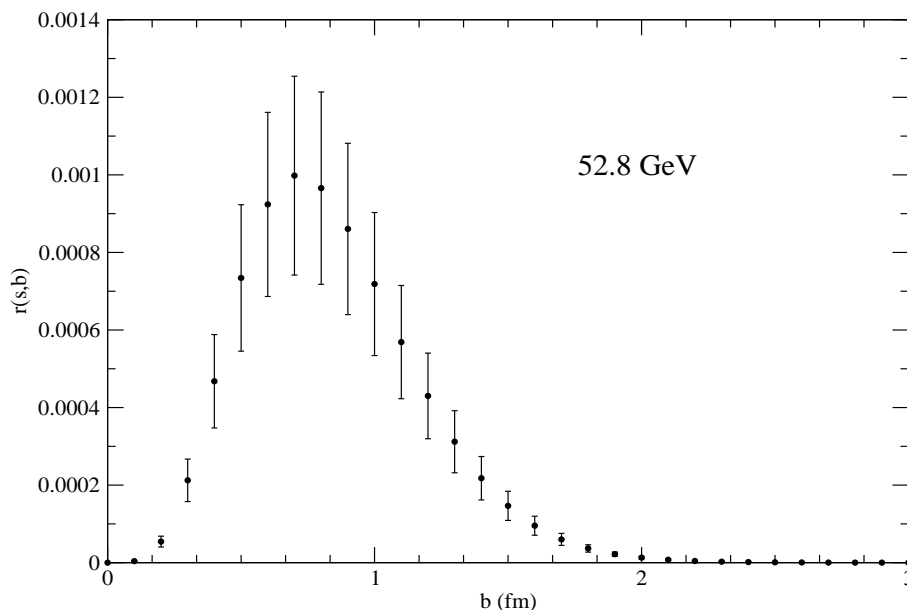


FIG. 6: Empirical points at 52.8 GeV for the ratio  $r(s, b)$  in Eq. (30) and uncertainties from error propagation.

feature in these results is the evidence of a zero (change of sign) in the opacity at finite values of the momentum transfer (around  $6.5 \text{ GeV}^2$ ), since even the uncertainties in  $q^8 \tilde{\Omega}(s, q)$  lie below the zero above the crossing point. Beyond this change of sign, the opacity goes smoothly to zero through negative values.

From the plots in Fig. 7 the position of the zero can be determined and the error involved estimated from the uncertainties in both sides of the zero position. The results for these zero positions in terms of the energy are displayed in Fig. 8. We note that in the previous analysis by Ávila and Menon with the constrained parametrization [9] there has been no evidence for a zero at  $19.4 \text{ GeV}$ . That is a consequence of the new compilation and normalization for this data set used here and described in detail in [6].

In order to obtain an analytical parametrization for the empirical points displayed in Fig. 7, we consider a general structure inspired in eikonal models with zero in the opacity function [70, 71] and based on the Glauber multiple diffraction formalism [72–74]. For fixed  $s$  we express:

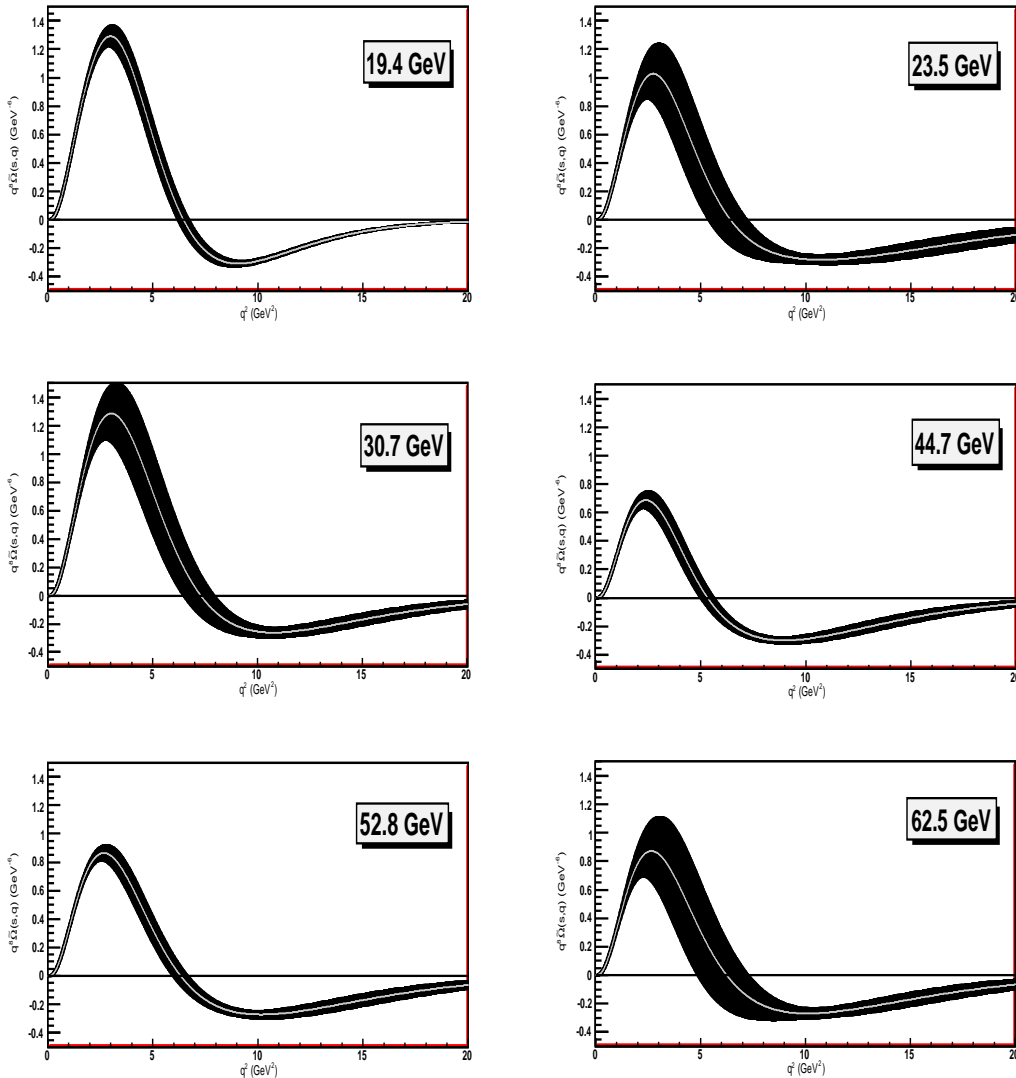


FIG. 7: Extracted opacity function in the momentum transfer space multiplied by  $q^8$  and uncertainty regions from error propagation.

$$\tilde{\Omega}(q) = CG^2(q)f(q), \quad (36)$$

with

$$G(q) = \frac{1}{(1 + q^2/\alpha^2)} \frac{1}{(1 + q^2/\beta^2)} \quad (37)$$

and

$$f(q) = \frac{1 - q^2/q_0^2}{1 + (q^2/q_0^2)^n}, \quad (38)$$

where  $C$ ,  $\alpha$ ,  $\beta$ ,  $q_0$  are free fit parameters and  $n$  a fixed integer. The change of sign (zero) in  $\tilde{\Omega}(q)$  is generated at  $q^2 = q_0^2$ .

These are general and useful formulas, since for different values of the integer  $n$  in  $f(q)$  they reproduce different model assumptions or empirical parametrization for the corresponding opacity function. In fact, for  $n = 1$  we have a structure used in the Bourrely, Soffer and Wu model [75–78], which we shall denote  $\tilde{\Omega}_{BSW}$ . The case  $n = 2$  corresponds to a modification in the BSW function, which appears in multiple diffraction [46, 49, 50] and hybrid [79] models and we shall denote  $\tilde{\Omega}_{mBSW}$  (standing for *modified*-BSW). At last, in the analysis by Ávila and Menon the value  $n = 4$  has been inferred on *empirical* basis and for that reason we shall denote  $\tilde{\Omega}_{empir}$ .

As before, in what follows we shall focus on the typical results obtained at  $\sqrt{s} = 52.8$  GeV. The point is to fit the empirical points with errors for the opacity function, as displayed in Fig. 7, through parametrization (36-38), in the cases  $n = 1$  ( $\tilde{\Omega}_{BSW}$ ),  $n = 2$  ( $\tilde{\Omega}_{mBSW}$ ) and  $n = 4$  ( $\tilde{\Omega}_{empir}$ ). In this procedure we have fixed the position of the zero to the empirical value at this energy, namely  $q_0^2 = 6.34$  GeV<sup>2</sup> and let free the parameters  $C$ ,  $\alpha^2$  and  $\beta^2$ . The results of the fits are displayed in Table V and Fig. 9, for  $q^8\tilde{\Omega}$  and also the modulus  $|\tilde{\Omega}|$ .

We conclude with this analysis that only  $\tilde{\Omega}_{empir}$  can reproduce the empirical points and in this case, from Table 5,  $\beta^2 \approx 1 + \alpha^2$  (a form factor discussed by G. Shaw, in the beginning of the seventies

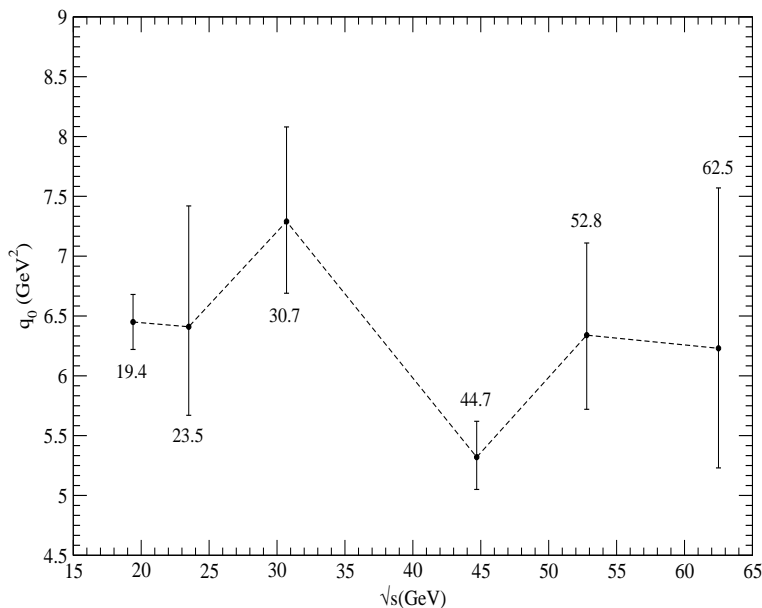


FIG. 8: Position of the zero in the opacity function extracted from the plots in Fig. 7 (see text) in terms of the energy. The dashed lines are drawn only to guide the eyes.

TABLE V: Results of the fits to the empirical points in Fig. 7 through Eqs. (36-38) at  $\sqrt{s} = 52.8$  GeV.

parameters	$\tilde{\Omega}_{BSW}$ ( $n = 1$ )	$\tilde{\Omega}_{mBSW}$ ( $n = 2$ )	$\tilde{\Omega}_{empir}$ ( $n = 4$ )
$C$ ( $\text{GeV}^{-2}$ )	$14.101 \pm 0.024$	$12.303 \pm 0.022$	$11.162 \pm 0.031$
$\alpha^2$ ( $\text{GeV}^2$ )	$0.5515 \pm 0.0024$	$0.6509 \pm 0.0040$	$0.4622 \pm 0.0041$
$\beta^2$ ( $\text{GeV}^2$ )	$0.5515 \pm 0.0024$	$0.6509 \pm 0.0040$	$1.431 \pm 0.018$
$\chi^2/\text{DOF}$	136	40	0.19

[80, 81]). These results are in plenty agreement with those obtained by Ávila and Menon through the constrained parametrization [9] and favor models with a zero in the eikonal (see [9] for more details).

## V. CONCLUSIONS AND FINAL REMARKS

The absence of a pure QCD treatment of the elastic hadron scattering and the lack of a widely accepted phenomenological approach to these processes, have motivated us to investigate the inverse problem, in the context of the impact parameter and eikonal representations. As commented along the paper two of the main problems with these model-independent analyses are: (1) we do not have information on the contributions from the real and imaginary parts of the amplitude beyond the forward direction; (2) the fits being non-linear have no unique solution. As a consequence, different kinds of solutions and contributions from the real and imaginary parts of the amplitude must be tested and reliable information should not strongly depend on the details of these solutions and contributions.

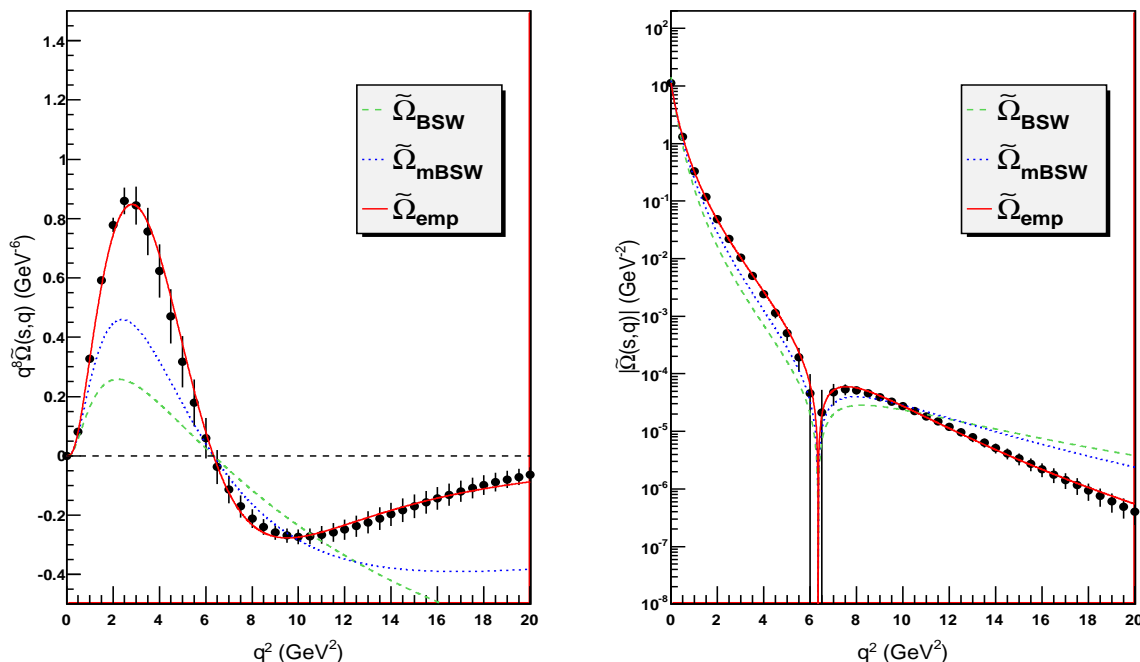


FIG. 9: Extracted opacity function at  $\sqrt{s} = 52.8$  GeV and parametrization through Eqs. (36-38) for different values of  $n$  in Eq. (38). Numerical and statistical information are shown in Table V.

With this strategy in mind, we have already developed two different empirical solutions for data reductions both statistically consistent and characterized by different contributions from the real and imaginary parts [6, 9]. Motivated by these differences we have discussed here the applicability of a representation for the Martin's formula without the full scaling property, which predicts also different contributions from the previous analyses.

A detailed review on the original derivation of this formula and critical comments on its further developments have been presented. The use of the proposed almost model-independent representation in empirical fits of the differential cross section data in the interval 19.4 GeV - 62.5 GeV has led to the following main conclusions:

- In the interval investigated, the experimental data on the differential cross sections at  $q^2 = 0$  and  $q^2 > 0.01 \text{ GeV}^2$  are quite well described.
- The extracted inelastic overlap function cannot be parametrized by one Gaussian distribution due to the tail effect, associated with the change of the slope in the differential cross section at small values of the momentum transfer. The empirical results indicate three Gaussian components whose sensitivity to variations of the energy increases from the central to the peripheral regions.
- The opacity function in the momentum transfer space, extracted through the conditioned expansion method, present a change of sign around  $6.5 \text{ GeV}^2$  in all sets analyzed. The empirical points are quite well described by a parametrization consisting of a product of two simple constrained poles ( $\beta^2 \approx 1 + \alpha^2$ ) by the function  $f(q)$  with zero and  $n=4$ .

Despite the promising aspects of the above results we stress that only a detailed comparative investigation, based on different empirical parametrization and solutions and aimed to identify results that are common to all the analyses, can bring new reliable insights for model developments and possible connections with QCD. A global critical review along these lines, collecting all our previous results and those presented here, are being prepared for a forthcoming communication.

### Acknowledgments

This research was supported by FAPESP (Contracts Nos. 11/00505-0, 09/50180-0, 07/05953-5).

- 
- [1] V. Barone and E. Predazzi, *High-Energy Particle Diffraction* (Spring-Verlag, Berlin, 2002).
  - [2] S. Donnachie, G. Dosch, P.V. Landshoff and O. Natchmann, *Pomeron Physics and QCD*, (Cambridge University Press, 2002).
  - [3] R. Fiore, L. L. Jenkovszky, R. Orava, E. Predazzi, A. Prokudin and O. Selyugin, *Int. J. Mod. Phys. A* **24**, 2551 (2009).
  - [4] <http://public.web.cern.ch/public/en/lhc/TOTEM-en.html>.
  - [5] J. Kaspar, TOTEM experiment: Elastic and total cross sections, in *Proc. 13th Int. Conf. Elastic and Diffractive Scattering*, eds. M. Deile, D. d'Enterria, A. De Roeck (DESY, Hamburg, 2010), p. 55.
  - [6] D.A. Fagundes, M.J. Menon and G.L.P. Silva, *Eur. Phys. J. C* **71**, 1637 (2011).
  - [7] D.A. Fagundes, M.J. Menon and G.L.P. Silva, Empirical Results for the Eikonal from Proton-Proton Elastic Scattering. in *Proc. XI Hadron Physics*, eds. M. Nielsen, F.S. Navarra and M.E. Bracco, AIP Conference Proceedings 1296 (AIP, Melville, 2010), p. 278.
  - [8] D.A. Fagundes and M.J. Menon, On a Model-independent Representation for the Real Part of the Elastic Hadron Amplitude, in *Proc. XI Hadron Physics*, eds. M. Nielsen, F.S. Navarra and M.E. Bracco, AIP Conference Proceedings 1296 (AIP, Melville, 2010), p. 282.
  - [9] R.F. Ávila and M.J. Menon, *Eur. Phys. J. C* **54**, 555 (2008).
  - [10] G.L.P. Silva, M.J. Menon and R.F. Ávila, *Int. J. Mod. Phys. E* **16**, 2923 (2007).
  - [11] R. F. Ávila, S. D. Campos, M. J. Menon, and J. Montanha, *Eur. Phys. J. C*, **47**, 171 (2006).
  - [12] P.A.S. Carvalho, A.F. Martini and M.J. Menon, *Eur. Phys. J. C* **39**, 359 (2005).
  - [13] P.A.S. Carvalho and M.J. Menon, *Phys. Rev. D* **56**, 7321 (1997).
  - [14] A. Martin, *Lett. Nuovo Cim.* **7**, 811 (1973).
  - [15] P. Valin, *Phys. Rep.* **203**, 233 (1991).

- [16] J. Fischer, *Phys. Rep.* **76**, 157 (1981).
- [17] S.M. Roy, *Phys. Rep.* **5**, 125 (1972).
- [18] R.J. Eden, *Rev. Mod. Phys.* **43**, 15 (1971).
- [19] A. Martin and G. Matthiae, Elastic Scattering and Total Cross Section, in *Proton-Antiproton Collider Physics*, eds. G. Altarelli and L. Di Lella, Advanced Series on Directions in High Energy Physics, Vol. 4 (World Scientific, Singapore, 1989), p. 45.
- [20] M.M Block and R. Cahn, *Rev. Mod. Phys.* **57**, 563 (1985)
- [21] M. Froissart, *Phys. Rev.* **123**, 1053 (1961).
- [22] A. Martin, *Phys. Rev.* **129**, 1432 (1963).
- [23] A. Martin, *Nuovo Cim.* **42**, 930 (1966).
- [24] G. Auberson, T. Kinoshita and A. Martin, *Phys. Rev. D* **3**, 3185 (1971).
- [25] J. Bros, H. Epstein and V. Glaser, *Nuovo Cimento* **31**, 1265 (1964).
- [26] J. Bros, H. Epstein and V. Glaser, *Com. Math. Phys.* **1**, 240 (1965).
- [27] R.J. Eden, *High Energy Collisions of Elementary Particles* (Cambridge University Press, Cambridge, 1967), Sect. 7.1.
- [28] J. Dias de Deus, *Nucl. Phys. B* **59**, 231 (1973).
- [29] A.J. Buras and J. Dias de Deus, *Nucl. Phys. B* **71**, 481 (1974).
- [30] J. Dias de Deus, *Nuovo Cim. A* **28**, 114 (1975).
- [31] J. Dias de Deus and P. Kroll, *Acta Physica Polonica B* **9**, 157 (1978).
- [32] N.V. Gribov and A.A. Migdal, *Sov. J. Nucl. Phys.* **8**, 583 (1969).
- [33] J.B. Bronzan, G.L. Kane and U.P. Sukhatme, *Phys. Lett. B* **49**, 272 (1974).
- [34] R.F. Ávila and M.J. Menon, *Nucl. Phys. A* **744**, 249 (2004).
- [35] UA4 Coll. (M. Bozzo *et al.*), *Phys. Lett. B* **147**, 392 (1984).
- [36] R. Henzi and P. Valin, *Phys. Lett. B* **132**, 443 (1983).
- [37] R. Henzi and P. Valin, *Phys. Lett. B* **149**, 234 (1984).
- [38] R. Henzi and P. Valin, *Phys. Lett. B* **160**, 167 (1985).
- [39] V. Kundrať and M. Lokajíček, *Phys. Rev. D*, **55**, 3221 (1997).
- [40] V. Kundrať and M. Lokajíček, *Phys. Lett. B* **232**, 263 (1989).
- [41] V. Kundrať and M. Lokajíček, *Phys. Rev. D*, **31**, 1045 (1985).
- [42] M. Kawasaki, T. Maehara and M. Yonezawa, *Phys. Rev. D*, **55**, 3225 (1997).
- [43] S.M. Roy, *Phys. Lett. B* **135**, 191 (1984).
- [44] J. Bellandi, R.J.M. Covelan, M.J. Menon and B.M. Pimentel, *Hadronic J.* **11**, 17 (1988).
- [45] A. Malecki, *Phys. Lett. B* **149**, 221 (1989).
- [46] M.J. Menon and B.M. Pimentel, *Hadronic J.* **13**, 325 (1990).
- [47] T.T. Chou and C.N. Yang, *Phys. Lett. B* **244**, 113 (1990).
- [48] T.T. Chou and C.N. Yang, *Phys. Lett. B* **128**, 457 (1983).
- [49] M.J. Menon, *Nucl. Phys. B. (Proc. Suppl.)*, **25**, 94 (1992).
- [50] M.J. Menon, *Can. J. Phys.*, **74**, 594 (1996).
- [51] M. Kawasaki, T. Maehara and M. Yonezawa, *Phys. Rev. D*, **47**, R3 (1993).
- [52] M. Kawasaki, T. Maehara and M. Yonezawa, *Phys. Rev. D*, **48**, 3098 (1993).
- [53] J. Dias de Deus and A.B. Pádua, *Phys. Lett. B* **317**, 428 (1993).
- [54] U. Amaldi and K.R. Schubert, *Nucl. Phys. B* **166**, 301 (1980).
- [55] E. Nagy *et al.*, *Nucl. Phys. B*, **150**, 221 (1979).
- [56] W. Faissler *et al.*, *Phys. Rev. D*, **23**, 33 (1981).
- [57] A. Donnachie and P.V. Landshoff, *Z. Phys. C*, **2**, 55 (1979).
- [58] A. Donnachie and P.V. Landshoff, *Phys. Lett. B* **387**, 637 (1996).
- [59] F. James, MINUIT - Function Minimization and Error Analysis (CERN, 2002)
- [60] P.R. Bevington and D.K. Robinson, *Data Reduction and Error Analysis for the Physical Sciences* (McGraw-Hill, Boston, Massachusetts, 1992).
- [61] A. Martin, *Phys. Lett. B* **404**, 137 (1997).
- [62] G.P. Lepage and S.J. Brodsky, *Phys. Rev. D*, **22**, 2157 (1980).
- [63] J.R. Cudell, A. Lengyel and E. Martynov, *Phys. Rev. D* **73**, 034008 (2006)
- [64] <http://nuclth02.phys.ulg.ac.be/cudell/data>
- [65] G. Alberi and G. Goggi, *Phys. Rep.* **74**, 1 (1981).
- [66] H.I. Miettinen, Impact Structure of Diffraction Scattering, in *Proc. 9th Rencontre de Moriond*, ed. J. Tran Than Van (Moriond Conference, 1974); preprint CERN-TH 1864 (1974).
- [67] A.S. Carroll *et al.*, *Phys. Lett. B*, **80**, 423 (1979).
- [68] A. Schiz *et al.*, *Phys. Rev. D*, **24**, 26 (1981).
- [69] F.S. Henyey, R.H. Tuan and G.L. Kane, *Nucl. Phys. B*, **70**, 445 (1974).
- [70] M.J. Menon, *Phys. Rev. D* **48**, 2007 (1993), Erratum-*ibid.* **51**, 1427 (1995).
- [71] A.F. Martini, M.J. Menon and D.S. Thober, *Phys. Rev. D* **54**, 2385 (1996).
- [72] R.J. Glauber, in *Lectures in Theoretical Physics*, edited by W. E. Brittin *et al.* (Interscience, New York, 1959) Vol. I, p.315.

- [73] W. Czyż and L.C. Maximon, *Ann. Phys. (N.Y.)* **52**, 59 (1969).
- [74] V. Franco and G.K. Varma, *Phys. Rev. C* **18**, 349 (1978).
- [75] C. Bourrely, J. Soffer and T.T. WU, *Eur. Phys. J. C* **28**, 97 (2003).
- [76] C. Bourrely, J. Soffer and T.T. WU, *Phys. Rev. D* **19**, 3249 (1979).
- [77] C. Bourrely, J. Soffer and T.T. WU, *Nucl. Phys.* **B247**, 15 (1984).
- [78] C. Bourrely, J. Soffer and T.T. WU, *Phys. Rev. Lett.* **54**, 757 (1985).
- [79] R.J.M. Covolan, P. Desgrolard, M. Giffon, L.L. Jenkovszky and E. Predazzi, *Z. Phys. C* **58**, 109 (1993).
- [80] G. Shaw, *Phys. Lett. B* **39**, 255 (1973).
- [81] M. Kac, *Nucl. Phys. B* **62**, 402 (1973).